Low Cost Thermal Σ–Δ Air Flow sensor

M. Domínguez*, F. Masana, V. Jiménez, S.Bermejo, J.Amirola, J. Ballester†, N. Fueyo† and L.Castañer

GDS, Electronic Engineering Dept., Technical University of Catalonia, UPC - Campus Nord Ed. C4, Jordi Girona 1-3
Barcelona Spain 08034, tel: 34934015679, Fax 34934016756, e-mail: mpumar@eel.upc.es
† Departamento de Ciencia y Tecnología de Materiales y Fluidos, Centro Politécnico Superior, Universidad de Zaragoza, María de Luna 3, 50015 Zaragoza, Spain. tel: 34976761000, Fax: 34976761882
e-mail:Norberto.Fueyo@posta.unizar.es

EDICS category: THER (4)

Abstract

This paper describes the design and optimization of a hot-wire air flowmeter. A low cost design of the packaging allows good thermal contact with the airflow as well as good thermal isolation between the hot and cold points. It is a compact solution which allows easy PCB mounting and adaptation to standard size small air pipes. The design has been optimized for low-cost applications. The sensor is read out by a thermal sigma-delta modulator. The dynamic range of this modulator has been extended by adding a constant power offset to its output. The fractal nature of the modulator response at low clock frequencies is also experimentally shown.

Keywords: Anemometer, flow sensor, thermal sigma-delta.

1.Introduction

Measurement of air flow is becoming important in low cost applications such as in wall hanged boilers, where the air incoming to the combustion chamber has to be monitored for safety purposes. Rather than a highly linear device, a good sensitivity sensor is required for these ON-OFF applications. The competitiveness of this market calls for low cost design provided it is able to detect airflow in a conduct between two points having a differential pressure under 100 Pa. The purpose of this paper is to describe a solution to this problem based on a hot-wire principle and thermal Σ–Δ (TΣΔ) modulation.

Silicon devices have been developed [1-4] in which a micromachined channel is built and where thermal detectors are integrated on top of bridges across the duct. This solution achieves short response times but is restricted to very small air ducts and subject to problems of dust deposition and duct occlusion. Moreover unit cost is generally high, and requires micromachining technology.

We presented [5-7] a new concept based on a lead-frame and built a water flow meter. This concept included a plastic packaging embodying two temperature sensors and two thermal-conducting paths from the water to the sensor. This solution proved to be simple and cost-effective even for medium size series. The purpose of this paper is to extend this concept to sensing air flow, introducing several design changes, and to extend the preliminary results shown in [11] providing more theoretical support.

This flowmeter, as well as that presented in [5-7], can be operated in open-loop mode (a constant power is delivered to the heater) or in closed-loop (a variable power is delivered to the heater so that the temperature difference between the hot and the cold points is kept constant). In the open-loop mode the magnitude upon which the airflow can be inferred is the temperature difference between the hot and the cold points. The cold point is kept at the temperature of the air inside the sensor, whereas the hot point temperature varies as a function of flow rate and is always above that of the cold point. This can represent a disadvantage because the time evolution of the sensor can be dominated by the largest thermal time constant of the structure. As any change in the airflow rate would cause the hot point to vary its temperature, the time response of the thermal circuit is very important.

This is avoided in the closed-loop mode because the hot point is kept at a constant temperature above that of the cold point. As long as the temperature of the airflow does not change the absolute temperatures of the hot and cold points remain constant and therefore the time constants of the thermal circuit of the sensor do not affect the time evolution of the sensor. We have adopted this solution because the time evolution of the temperature of the airflow inside the sensor is expected to be slower than that of the thermal structure of the sensor.

A key issue is the thermal isolation between the hot and cold points. It is necessary to achieve a good sensitivity and also to ensure that the cold point remains at the temperature of the air. If the temperature at the cold point is affected by the power injected by the heater, then both temperature sensors, working in the closed-loop mode, would follow the variations of the airflow, with the associated time-constants of the thermal structure.

We have chosen a thermal sigma-delta modulator as closed-loop control circuit [3, 6-11]. This modulator provides maximum power efficiency (the heater is totally ON or totally OFF) and also provides a robust digital conversion. It is interesting to note that off-the-shelf sigma-delta converters might provide a good and inexpensive A/D conversion of the sensor working in the open loop mode. However working in closed-loop mode needs an external circuit to force a constant temperature difference between the hot and cold points. The main advantage of thermal sigma-delta modulation is that it fulfills both aims at the same time: it provides a robust A/D conversion and also allows the sensor to work in the constant temperature difference mode.

In this paper we propose a simple change in the standard circuit topology which allows an increase of the output dynamic range of the sensor. We also show some experimental evidence of fractal nature of the response of the modulator for low clock frequencies, as predicted in [9]. Although the thermal sigma-delta modulator conceptually does not differ from other sigma-delta modulators, this intrinsic aspect of the operation of the modulator is experimentally shown for the first time in a flow sensor device.

Numerical simulations have been carried out which show that the main assumptions of the design have been fulfilled: turbulent flow forced by two transversal thermal contacts in the middle of the fluid and acceptable thermal isolation between the hot and cold points.

2. Sensor Description

The concept of this sensor is schematically depicted in Figure 1, where it can be seen the inner air duct from input to output, and somewhere in the path, the air finds two metallic transversal pins. These pins are in the opposite face of the lead frame to which the temperature sensors are bonded. This is more clearly seen in Figure 2 where a cross-section is shown. The inner duct has a slightly conical shape to facilitate the moulding process of the packaging. As can be seen no direct contact exists between the sensor dice and the air. Instead, the thermal contact is made through the high thermal conductivity lead-frame, thus extremely simplifying packaging and also giving robustness and long-term life against corrosion.

The temperature sensors are bipolar junction common-collector transistor arrays, essentially the same described in [6], in which the hot point sensor is surrounded by a NiCr heating resistor. A scheme of the lead-frame is shown in fig. 3. Top and bottom sacrificial bars provide firmness in the process of manipulation and epoxy transfer to the mould and must be cut prior to sensor use to allow electrical contact with dice pads.

The sensor can be separated in two parts: a bulk where dice and lead-frame are located and a lid, which prior to mounting the sensor gives access to the lead-frame islands where the hot and cold temperature sensors have been fixed. This allows soldering small terminals to the dice islands to enhance the thermal contact between temperature sensors and fluid. These terminals serve a two-fold purpose. First, they serve to enhance the heat conduction from the heater and the temperature sensors to the airflow inside the sensor. Second, as an obstacle in the middle of the inner duct of the sensor they help to produce a turbulent flow, which is necessary to have a truly convection heat transfer with a strong dependency from flow velocity.

Special attention has been paid to the design of the dice islands in order to ensure good thermal contact and simultaneously reducing the time constants of the thermal circuit of the structure. Both islands have been separated almost 1 cm and whenever possible it has been avoided the presence of copper lines between them. Also the copper islands upon which the dice are located are tangent to the inner channel of the sensor (see figure 2) and are located immediately below the transversal contacts, thus reducing the thermal resistance to the airflow inside the sensor. Also, the copper lead-frame thickness has been reduced to 0.2 mm. With all this, a stronger thermal coupling with the airflow is accomplished and the thermal resistance between the hot and cold points is increased.

A photograph of the sensor is shown in figure 4. Dummy bars have been removed and six terminals are accessible: 4 for temperature sensors (2 for each, hot and cold point) and 2 more which contact the heating resistor.

3. Sensor modeling

Numerical simulations of the structure have been carried out using a CFD tool, FLUENT, and good agreement between experimental measurements and simulations has been achieved. The purpose of these simulations is to verify that the main assumptions of the design are accomplished: (a) good thermal isolation between hot and cold points and (b) turbulent flow forced by the transversal thermal contacts. Simulations are validated by comparing the numerical results obtained for different flows with experimental measurements. The sensor was simulated in the open-loop mode with a constant delivered power to the heater of 150mW.

The complete simulated geometry can be observed in figure 1. The epoxy structure has been made almost transparent for the sake of clarity and only the air channel along with chips, lead-frame and thermal transversal contacts have been highlighted. The simulated geometry includes epoxy packaging, copper lead-frame, temperature sensors chips, transversal thermal contacts and the inner air channel.

A list of the physical properties of the simulated materials is shown in Table I.

Material	**Density (Kg/m^3)**	**Cp (J/KgK)**	**Thermal Conductivity (W/mK)**	**Dynamic Viscosity (Kg/ms)**
Copper	8993	385	401	-
Silicon	2330	712	150	-
Epoxy MG15 Hysol	2000	1200	0.6	-
Air	1.225	1006.3	0.0242	1.7894e-5

Table I: Physical properties of the simulated materials of the sensor.

The process to obtain a suitable set of boundary conditions for the fluid flow at the inlet and outlet of the sensor working at different pressures has been the following:

a) The simulation of a longer pipe, of the same diameter as the sensor, to obtain the actual developed flow at the inlet to the sensor. The main input for this step is the actual flow rate (l/min.) for a given pressure at the plug-ins of the sensor. The relation between the air mass flow and pressure is shown in figure 5.

b) Once the developed-flow velocity-profile is obtained, it is used as the inlet boundary condition to the simulation of the whole structure of the sensor, which includes packaging, copper lead-frame along with silicon dice. As velocities are specified at the inlet, an outflow boundary condition is used at the output. The boundary conditions used at the outlet are the usual zero-gradient ones, constructed by extrapolating the flow conditions at the exit plane.

The results of the simulations show that the two main hypotheses are fulfilled. Firstly, good thermal isolation has been achieved between the cold point and the hot point. Secondly, the presence of the thermal transversal contacts enhances the production of turbulence, and hence mixing and heat transfer. The calculated temperature and velocity fields are shown in figures 6 and 7.

Temperature contours for ΔP =100 Pa, can be seen in figure 6. The inner volume of the sensor presents an almost constant temperature value of 25 ºC, except of course in the region next to the hot point and its transversal contact. The cold point remains at 25 ºC.

The velocity vectors for the same flow can be observed in figure 7. They show a flow velocity increase in the middle of the sensor due to the conical shape of the inner duct of the sensor. The presence of the transversal contacts creates turbulence just past the cold point. This ensures that heat transfer to the fluid is enhanced at the hot point.

Table II shows good agreement between numerical results and experimental measurements for several flow-rates that cover the full operational range of the sensor.

Pressure (Pa)	Hot point T (K)	Cold point T (K)	Calculated ΔT (K)	Experimental ΔT (K)
0	310.4	298.00	12.40	11.09
20	309.49	298.00	11.49	10.66
40	309.25	298.00	11.25	10.17
60	309.15	298.00	11.15	9.92
80	309.09	298.00	11.09	9.71
100	308.99	298.00	10.99	9.54

Table II: Comparison between simulated and experimental temperature increments for different flow rates.

4. Thermal Σ–Δ modulator dynamic range enhancement

A thermal sigma-delta modulator was chosen to close the loop in the constant temperature mode. A schematic of the general topology for this circuit can be found in figure 9 (for δ=0) [4,9]. A pulsed power source is switched ON and OFF and the feedback loop keeps the integrator output close to the voltage offset (V_{off}) set at the input of the comparator. Ground temperature is that of the cold point. It was shown in [9] that the signal at the output of an M-pole thermal filter can be approximated by its DC value (y_{DC}) for a sufficiently high working frequency of the sigma-delta loop (the same result assumed for frequencies above the filter cut-off frequency in [10]). If we define the AC component of the thermal integrator output (y_{AC}) as the maximum amplitude of the variations of the thermal integrator output with respect to its DC value, then, for any given value of the average number of '1's at the output of the integrator, it is possible to find a sufficiently high frequency above which the AC component of the signal is smaller than any desired value.

The same result can be easily reached for thermal circuits having a continuous time constant density as defined in [12]. It is interesting to work out the case where a non-discrete time constant density is found because the transfer function (h(t)) of any thermal sensor can be more generally expressed in those terms, being in fact the lumped network an approximation to the actual thermal response of the sensor. This is a generalization of the theory described in [9]. The representation of the transfer function of the thermal filter (h(t)) as a function of a time constant density is [12]:

$$h(t) = \int_{-\infty}^{+\infty} \frac{R(\zeta)}{e^{\zeta}} \exp(-t / e^{\zeta}) d\zeta \tag{1}$$

where a logarithmic time-constant variable (ζ) has been used and R(ζ) is the time-constant density defined as a function of ζ. Then, the DC component of the output of the integrator as a function of the average number of '1's (λ^1) at the output of sigma-delta modulator is:

$$y_{DC} = \lambda^1 \alpha P_c H(0) = \lambda^1 \alpha P_c \int_{-\infty}^{+\infty} R(\zeta) d\zeta = \lambda^1 \alpha P_c \beta$$

$$\beta := \int_{-\infty}^{+\infty} R(\zeta) d\zeta$$

(2)

where α (mV/ºC) is the temperature coefficient of both temperature sensors, P_c is the injected heat power when the controlled source is ON and H(0) is the Fourier Transform of h(t) for zero frequency. The term $\lambda^1 P_c$ is the average power delivered to the thermal filter. The maximum AC component of the signal at the output of the thermal can be found after algebraic manipulation to be:

$$y_{AC} \leq \frac{1}{6 f_0 \lambda^1} \int_{-\infty}^{\infty} \frac{|R(\xi)|}{e^{\xi}} d\xi, \qquad 0 < \lambda^1 \leq \frac{1}{2}$$

(3)

$$y_{AC} \leq \frac{1}{6 f_0 (1-\lambda^1)} \int_{-\infty}^{\infty} \frac{|R(\xi)|}{e^{\xi}} d\xi, \qquad \frac{1}{2} \leq \lambda^1 < 1$$

(4)

where f_0 is the clock frequency of the modulator. Assuming the finiteness of the above integrals, which is expected for most practical thermal circuits as they always act as strong low-pass filters (first time constant greater than 0), Equations in (3) and (4) show that for every value of λ^1 it is possible to work at a sufficiently high frequency such that the AC component at the output of the thermal integrator is smaller than any desired small value. In fact it is advisable to have a small AC component because if not, a fractal response is expected [9] and then, for some given voltage offsets, small variations of flow might not be detected at the output of the modulator. This implies that in general the temperature difference between the hot and cold points can be approximated by Voff/α for a sufficiently high frequency, and hence the sigma-delta modulator is indeed closing the loop. Although the above result is known for standard first-order sigma-delta modulators [8], the derivation above shows that the same result is found in the case where a thermal circuit performs the functions of integrator (a non-ideal integrator).

In Eq. 2 the β factor is a function of flow velocity. If only a convection term is considered, β represents the convection resistance. The dynamic range output can be calculated as follows:

$$\lambda^1 \approx \frac{Voff}{\alpha P_c \beta}, \qquad \lambda^1_{\max} = \frac{Voff}{\alpha P_c \beta_{min}} (maximum\ flow) \quad \lambda^1_{\min} = \frac{Voff}{\alpha P_c \beta_{max}} (zero\ flow)$$
$$\Delta\lambda^1 = \lambda^1_{max} - \lambda^1_{min} = \frac{Voff}{\alpha P_c}\left(\frac{1}{\beta_{min}} - \frac{1}{\beta_{max}}\right) \tag{5}$$

In order to maximize the span of the output of the sensor and hence its sensitivity, the voltage offset must be set at a value where in presence of maximum flow the output of the modulator is close to 1. Typically a 80-90% of the maximum output is selected to avoid saturation. Then, as flow decreases the modulator output will also decrease down to the λ^1_{min} value.

It is interesting to note that the total output range is independent of P_c. In order to achieve the maximum output range, λ^1_{max} will always have a value close to 1. Then:

$$\lambda^1_{\max} = \frac{Voff}{\alpha P_c \beta_{min}} \approx 1 \quad \Rightarrow \quad \Delta\lambda^1 = 1 - \frac{\beta_{min}}{\beta_{max}} \tag{6}$$

As can be seen the output range depends strictly on the sensor sensitivity and therefore is independent of the maximum power applied (P_c) which only acts as a normalization factor.

Only practical values of 20% of the full range were reached with our sensor in the range of 0-100 Pa. To achieve a greater span a constant power source has been added to the modulator. The criteria we have followed to properly size this new constant power source is to keep the total maximum power delivered to the hot point constant and equal to P_c, so:

$$\begin{aligned}\text{Pulsed power source} &= (1\text{-}\delta)P_c \\ \text{Constant power source} &= \delta P_c\end{aligned} \tag{7}$$

with $0<\delta<1$. Now the value of P_c in equation (2) must be replaced by:

$$y_{DC} = \lambda^1(1-\delta)\alpha P_c\beta + \delta\alpha P_c\beta \approx Voff \tag{8}$$

And then:

$$\lambda^1_{min} = \frac{Voff}{\alpha P_c}\frac{1}{(1-\delta)\beta_{max}} - \frac{\delta}{1-\delta}, \quad \lambda^1_{max} = \frac{Voff}{\alpha P_c}\frac{1}{(1-\delta)\beta_{min}} - \frac{\delta}{1-\delta} \tag{9}$$

It can be seen that now the dynamic range depends on δ. By choosing a correct value for δ it is possible to modify the output range of the sensor up to the 100%. It is not advisable to reach the 100% span because any flow instabilities would cause saturation near maximum flow. This must be avoided because if the sensor is saturated at the 100% (i.e. the heater is always ON) the closed-loop would be no longer enforced by the thermal sigma-delta modulator and the sensor would operate in open-loop mode and thus its time evolution would be affected by the largest time constant of the thermal circuit of the sensor.

An example of the evolution of the output range as a function of δ for $Voff/(\alpha P_c\beta_{min})$=90% and $Voff/(\alpha P_c\beta_{max})$=70% is given in figure 10.

In the usual configuration of a thermal $\Sigma-\Delta$ modulator configuration, a D flip-flop switches ON and OFF a driver transistor of the heater resistor. By adding a parallel resistor (R_{adjust}) to the transistor in series with the heater resistor the constant power source can be easily implemented. Then the δ factor can be adjusted as follows:

$$\delta = \frac{R_{heater}}{R_{adjust} + R_{heater}} \tag{10}$$

5. Results

Several devices were fabricated and extensive measurements performed. The modulator clock frequency is 3KHz and the maximum injected power (P_c) 150mW. During this measurements the output of the modulator is decimated with a 255 point square filter, using integer arithmetic which can be easily implemented in any low cost microcontroller. These samples are filtered with another 10 point square filter to give the final output. Typically, the temperature difference between the hot and cold points is 10ºC approximately. The ambient temperature is 20ºC and the temperature of the air inside the sensor is also 20ºC approximately. Sensor resolution for stationary measurements has been estimated to be ∀5%, approximately.

The introduction of the thermal transversal contacts and the new range enhancement method are found to increase the dynamic range of the sensor, enhancing then the overall behavior of the sensor (see figure 11). It can be observed that the introduction of the range enhancement strategy makes the sensor follow the behavior predicted in figure 10. Without transversal thermal contacts and without range enhancement the output range is approximately 8% (between the 86% and 94% of the output). With the inclusion of the transversal contacts the range goes up to 20% and once the range has been augmented with the proposed strategy it goes up to 63% (from 7 to 70%). It has been explicitly avoided the saturation of the modulator for all the pressure range, thus preventing the sensor from falling into the open-loop mode due to any flow instability near the maximum flow rate.

Figure 12 shows the response to a step function (from 0 Pa to 100 Pa). The response speed is of 60s approximately although a certain heating of the cold point can be observed for zero flow. This is the reason why sometimes down-step flow transients may produce variations of the absolute temperatures of both hot and cold points. The hot point suffers variations because the sensor is working in the closed-loop mode and the hot point is following the variations of the cold point (plus the forced temperature increment).

Figure 13 shows a measurement of the power spectrum density of the bit stream at the output of the modulator. The noise shaping characteristic behavior of sigma-delta modulation is clearly visible. An idle tone can be observed at 700Hz but is totally out of band.

5.1Non-linear effects of Σ–Δ modulation

The effects of leaky integrators on sigma-delta modulation have been studied intensely in the past. The fractal nature of the transfer function of the modulator has been proved to be that of the "Devil's Staircase", [13-14]. But what for standard sigma-delta designers is a curiosity because it is possible to build an almost perfect integrator in the working clock frequency range of the modulator, is a far more complicated issue for thermal sensors designers. In this case, the integrator belongs to the thermal domain. That means the thermal equivalent circuit of the sensor itself. No easy optimizations can be made because those changes would imply a new packaging, sensor structure, etc. Sensor designers solve this problem by avoiding the low frequency range where the non-idealities of the integrator are more relevant and produce the fractal response of the modulator. With the purpose to illustrate the fractal behaviour figure 14 shows the output of the sensor for zero flow at a very low frequency (75Hz) compared with the operating frequency, as a function of the offset voltage. The response is very similar to that of the 'Devil's staircase': the main "plateau" can be seen at 50% of the output and duplicates of that at other levels (20%, 33%, 66% and 80% approximately). The graph is smoothed due the noise of the sensor, which acts as a dithering signal. The fractal response of the sensor is not observed for frequencies above 200-300Hz.

For most practical sensor circuits, a trade-off exists between having a very small AC component and having an acceptable SNR at the output of the thermal integrator. A small AC component is required to avoid the fractal response and to ensure an almost constant temperature difference between the hot and cold points. On the other hand, having a small AC component means that the variations of the signal at the output of the temperature sensors are very small. Cross-talk problems between the power line (heater) and the temperature sensor of the hot point can then arise. Three components must be balanced: first, the clock frequency of the modulator; second, the SNR present at the output of the thermal integrator; and third, the decimating filter in the digital domain. Avoiding the fractal and ensuring a small AC component force a high clock frequency that can produce cross-talk and hence a decreasing of the SNR at the output of the integrator. This can be compensated by a strong decimation digital filtering. In our case, we have adopted an intermediate frequency (3 KHz), in comparison with the 8192Hz of [3] for example, and a strong decimation filtering in the digital domain.

With respect to the fractal response, the most dangerous problem comes from the shortest time constant of the thermal circuit. When a step function is applied at the heater, the temperature sensor of the hot point senses a local heating and afterwards senses the heating of the part of the sensor in contact with the airflow. In the sensor of [6,15] two time constants could be found: one of 1.5 ms (not related with flow) and other of 1.5s (related with flow). The first was due to the local heating of the hot die, the second was due to the heating of the hot pin in contact with the water flow. A frequency of 1KHz was used and the high frequency components of the bit stream were filtered by the second time constant. The AC component of the signal at the output of the integrator was mainly due to the first time constant and the second time constant generated a DC voltage superimposed to the voltage offset of the circuit. Then, the time constant that fixes the minimum required frequency of the modulator is always the shortest.

6. Conclusions

A novel air-flow anemometer is presented. It is a compact design which opts for making the thermal contact with fluid through the lead-frame thus providing a low-cost solution. The numerical modeling of the sensor verifies that the thermal coupling between the hot and the cold point is acceptable and that turbulence formation is enhanced by the transversal thermal contacts which also increase the overall sensitivity of the sensor. A new variation of the standard thermal sigma-delta circuit topology has also been proposed which allows an optimization of the output range of the sensor. Experimental evidence of the fractal response of the sensor, for low clock frequencies of the thermal sigma-delta modulator, is also given.

References

[1] Lammerink, T.S.J., Tas, N.R., Krijnen, G.J.M., Elwenspoek, M. “A new class of thermal flow sensors using $\Delta T=0$ as a control signal”, Micro Electro Mechanical Systems, MEMS 2000, p. 525-530, 2000.

[2] Mullins, M., Bayford, R., Van Putten, A., Butcher, J., “Design and fabrication of single-chip intelligent silicon thermal flow sensors in standard CMOS technology “, IEE Colloquium on Advances in Sensors for Fluid Flow Measurement, p. 14/1-14/4, 1996.

[3] Makinwa, K.A.A., Huijsing, J.H., “A smart wind-sensor based on thermal sigma-delta modulation”, Transducers’01, 2001.

[4] Verhoeven, H-J, Huijsing, J.H., "Design of integrated thermal flow sensors using thermal sigma-delta modulation", Sensors & Actuators A, Vol. 52, p. 198-202, 1996.

[5] Castañer, L., Jiménez, V., Domínguez, M., Masana, F., Rodríguez, A., "Flow measurement hits home. Using MEMS technology for flow sensing in home appliances", IEEE Circuits & Devices, Vol. 13, No. 1, pag. 14-18, 1997.

[6] Castañer, L., Jiménez, V., Domínguez, M., Masana, F., Rodríguez, A., "A conduction-convection design for liquid flow sensing", Sensors & Actuators A,Vol. 66, p. 131-137, 1998.

[7] Castañer, L., Jiménez, V., Domínguez, M., Masana, F., Rodríguez, A., "Design and fabrication of a low cost water flow meter", IEEE-Transducers-97, p. 159-162, 1997.

[8] Candy, J.C., Temes, G.C., "Oversampling Delta-Sigma Data Converters : Theory, Design, and Simulation", John Wiley & Sons, 1992.

[9] Domínguez, M., Castañer, L., "Bounding of thermal Σ–Δ output for sensors", ISCAS'99, p. II.244-II.247, 1999.

[10] Makinwa, K.A.A.; Huijsing, J.H., "Constant power operation of a two-dimensional flow sensor using thermal sigma delta modulation techniques", IMTC 2001, Vol. 3, p. 1577-1580, 2001.

[11] Domínguez, M., Masana, F., Jiménez, V., Bermejo, S., Amírola, J., Castañer, L., "A novel low cost lead-frame air flow anemometer", Transducers-2001, Vol. 2, p. 1468-1471, Munich, June 2001.

[12] Székely, V., "On the representation of infinite-length distributed RC one-ports", IEEE Transactions on Circuits and Systems, Vol. 38, No. 7, p. 711-719, 1991.

[13] Feely, O.,Chua, L.O., "The Effect of Integrator Leak in S-D Modulation", IEEE Trans. on Circuits and Systems, Vol. 38, No. 13, p. 1293-1305, 1991.

[14] Kennedy, M.P., Krieg, K.R., Chua, L.O., "The devil's staircase: The electrical engineer's fractal", IEEE Trans. Circuits and Systems, Vol. 36, p. 1133-39, 1989.

[15] Dominguez, M., PhD dissertation, Universitat Politècnica de Catalunya, 1997.

List of Figure Captions

Fig. 1: Structure of the sensor (flow channel diameter: 2mm).

Fig. 2: Sensor cross-section. Silicon dice are tangent to the inner channel (transversal thermal contacts dimensions: 1x1.5x0.2 mm^3).

Fig. 3: Lead-frame structure.

Fig. 4: Photograph of the sensor.

Fig. 5: Air mass flow in the sensor for given pressures

Fig. 6: Temperature contours (in K) in the sensor for a pressure of 100Pa and 150mW. The position of the decimal dot indicates the line to which the value applies.

Fig. 7: Flow pattern (velocity vectors) in the sensor for a pressure of 100Pa.

Fig. 8: Comparison between simulated and experimental temperature increments for different flow rates.

Fig. 9: General thermal Sigma-Delta topology.

Fig. 10: λ^1_{max}, λ^1_{min} evolution as functions of δ for $V_{off}/(\alpha P_c \beta_{min})$=90% and $V_{off}/(\alpha P_c \beta_{max})$=70%.

Fig. 11: Stationary measurements with transversal thermal contacts and range enhancement, and without transversal thermal contacts and without range enhancement.

Fig. 12: Sensor response to a step function (pressure from 0 Pa to 100Pa).

Fig. 13: Welch power spectrum density estimate of the bit-stream at the output of the modulator (32K samples, 3KHz modulator clock frequency).

Fig. 14: Response of the sensor at 0 flow at 75Hz as a function of voltage offset.

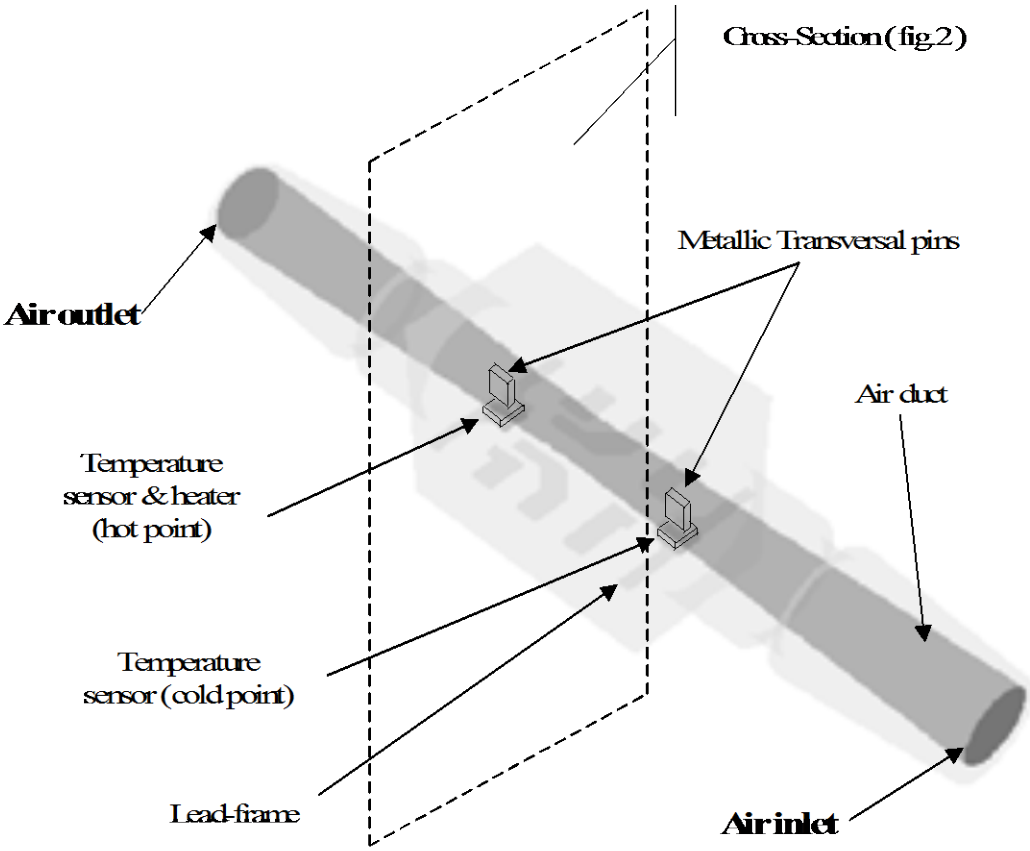
Cross-Section (fig.2)
Metallic Transversal pins
Air outlet
Air duct
Temperature
sensor & heater
(hot point)
Temperature
sensor (cold point)
Lead-frame
Air inlet

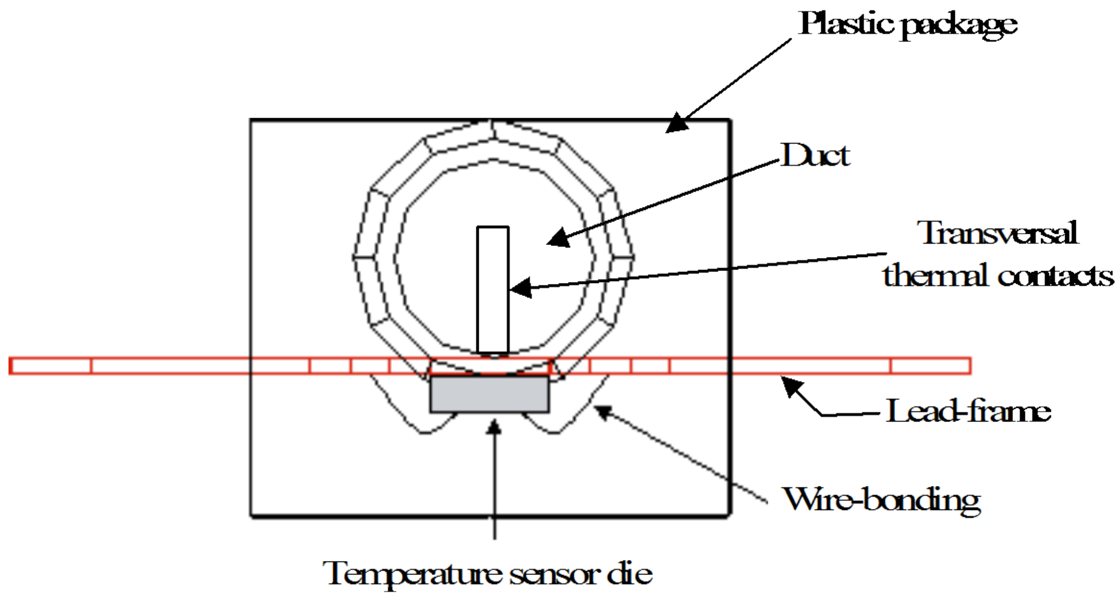
Plastic package
Duct
Transversal
thermal contacts
Lead-frame
Wire-bonding
Temperature sensor die

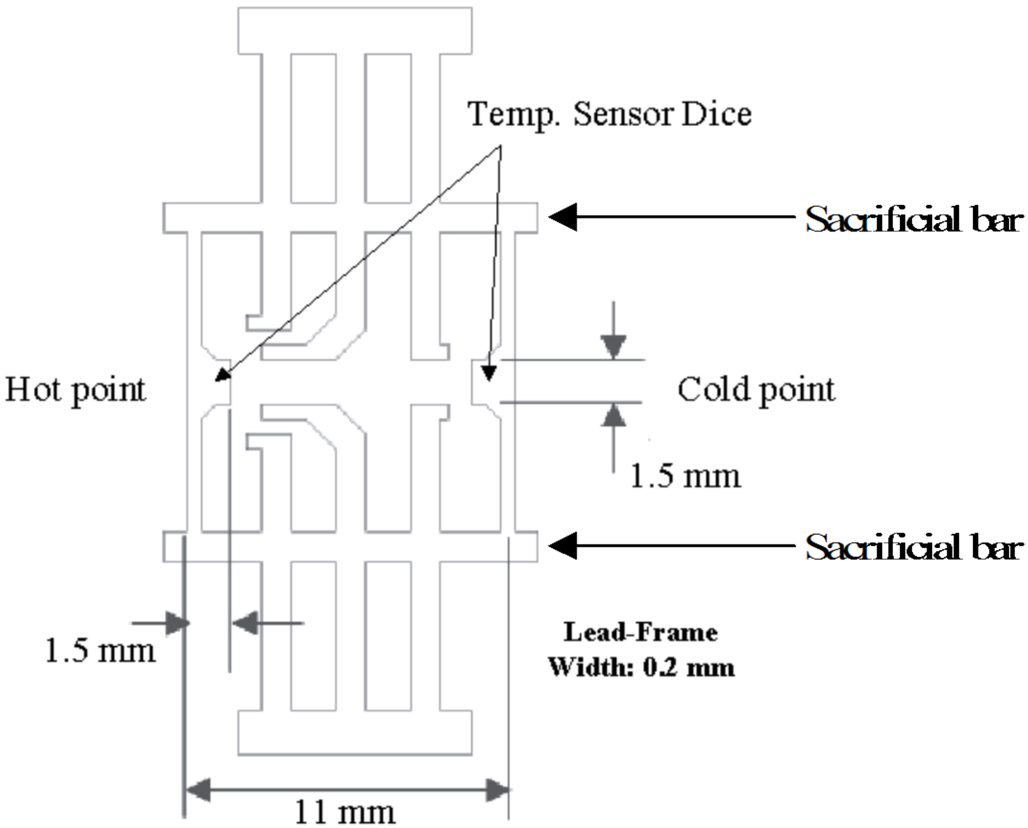
Temp. Sensor Dice
Sacrificial bar
Hot point
Cold point
1.5 mm
Sacrificial bar
1.5 mm
Lead-Frame
Width: 0.2 mm
11 mm

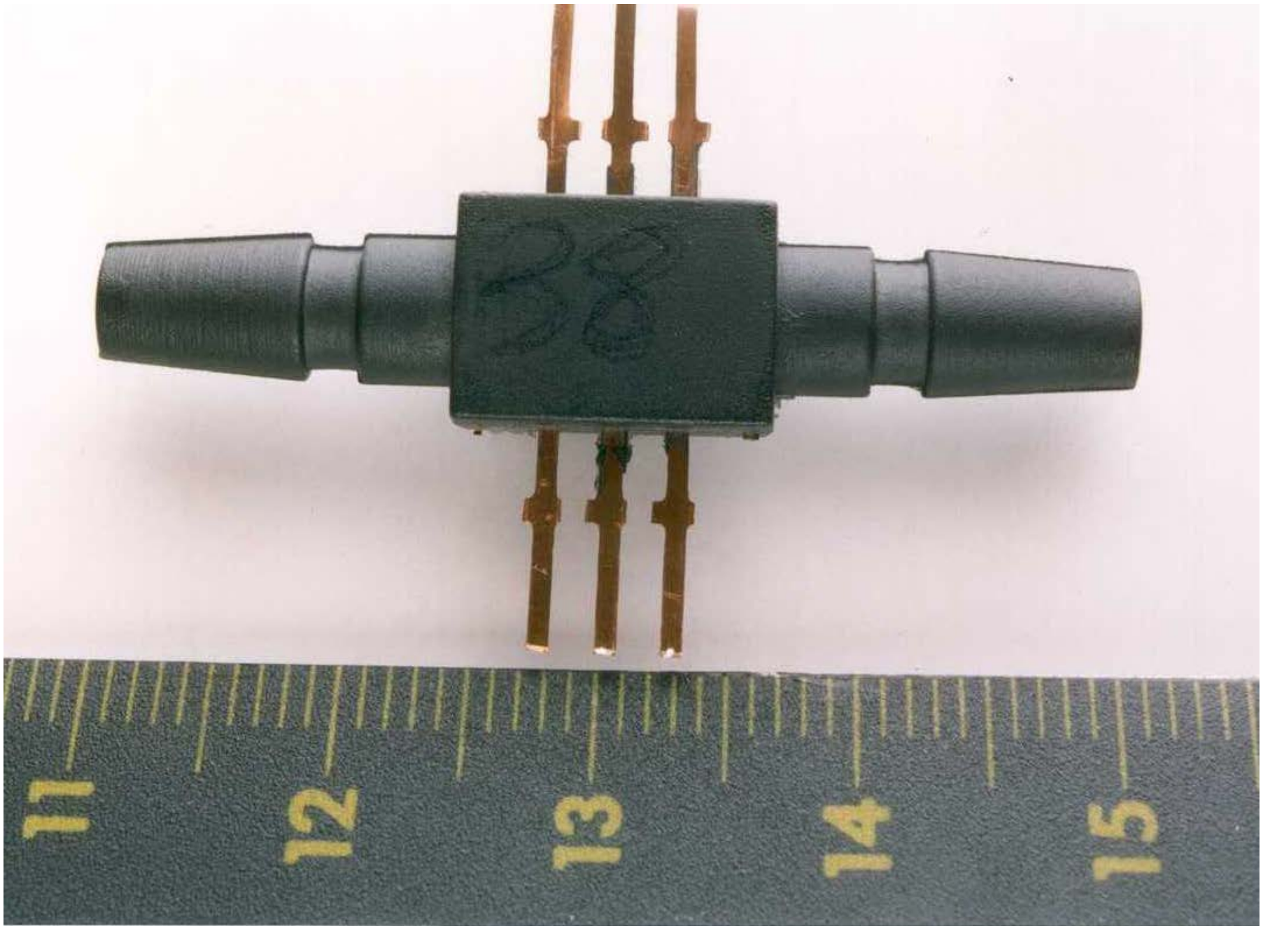
38
11
12
13
14
15

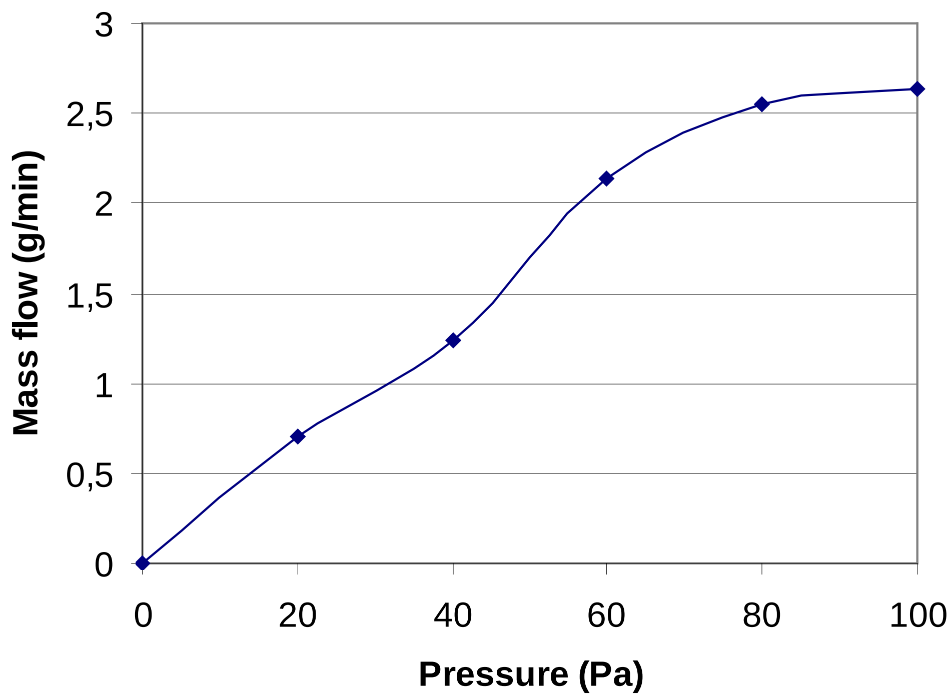
3
2,5
2
1,5
1
0,5
0
Mass flow (g/min)
0
20
40
60
80
100
Pressure (Pa)

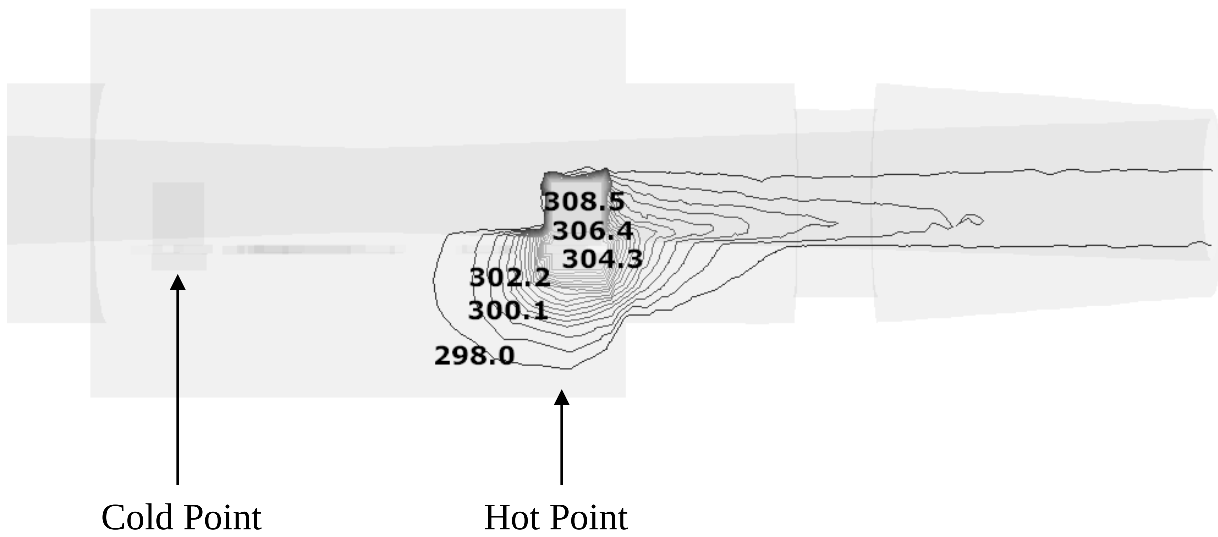
308.5
306.4
304.3
302.2
300.1
298.0
Cold Point
Hot Point

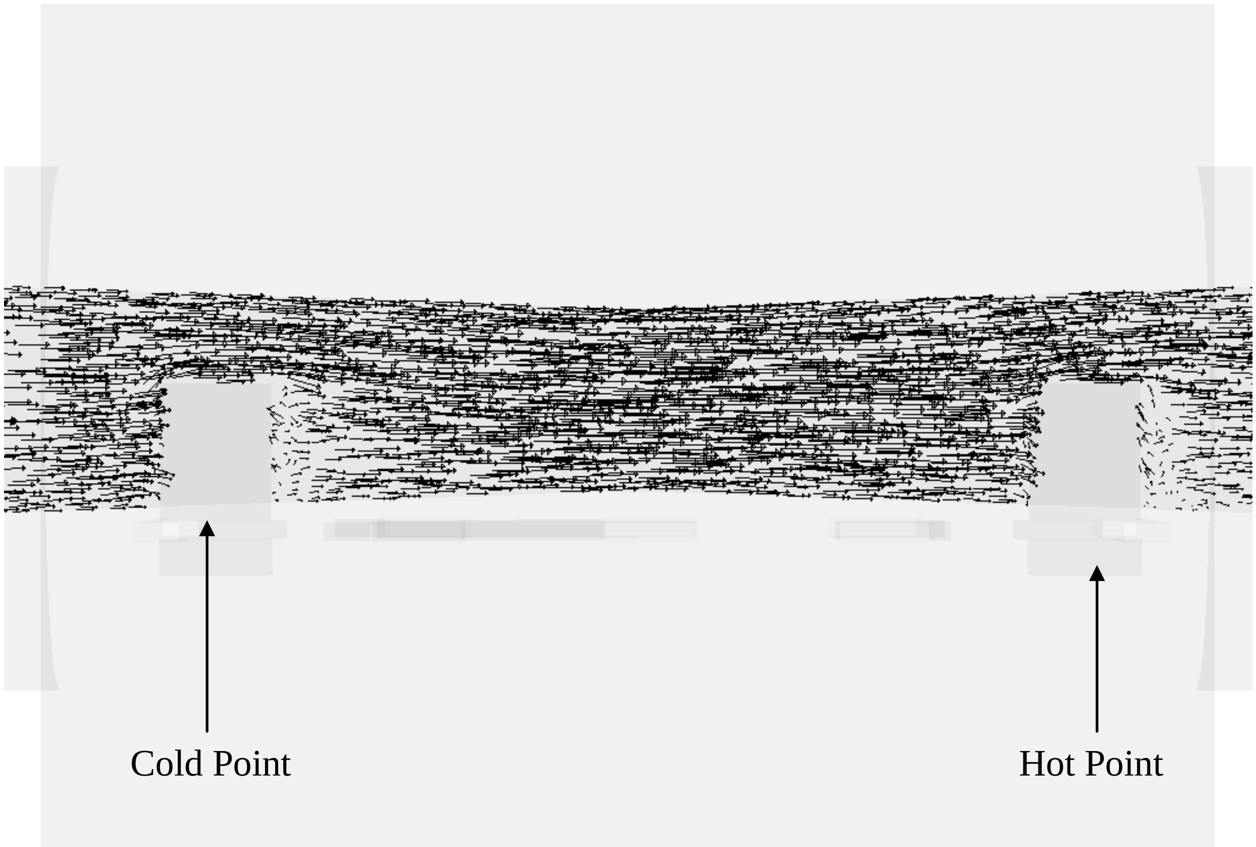

Cold Point
Hot Point

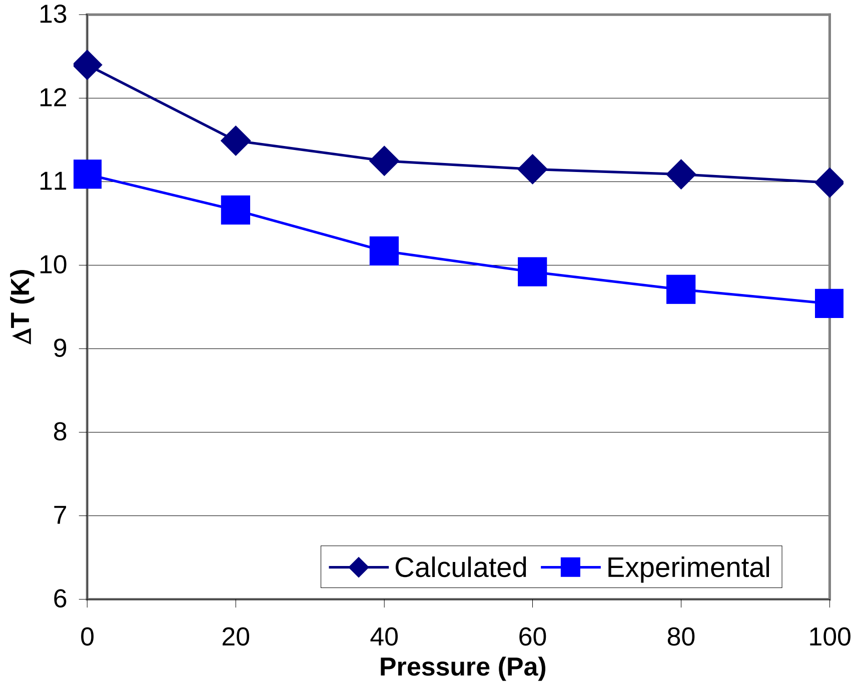

13
12
11
10
9
8
7
6
ΔT (K)
Calculated
Experimental
0
20
40
60
80
100
Pressure (Pa)

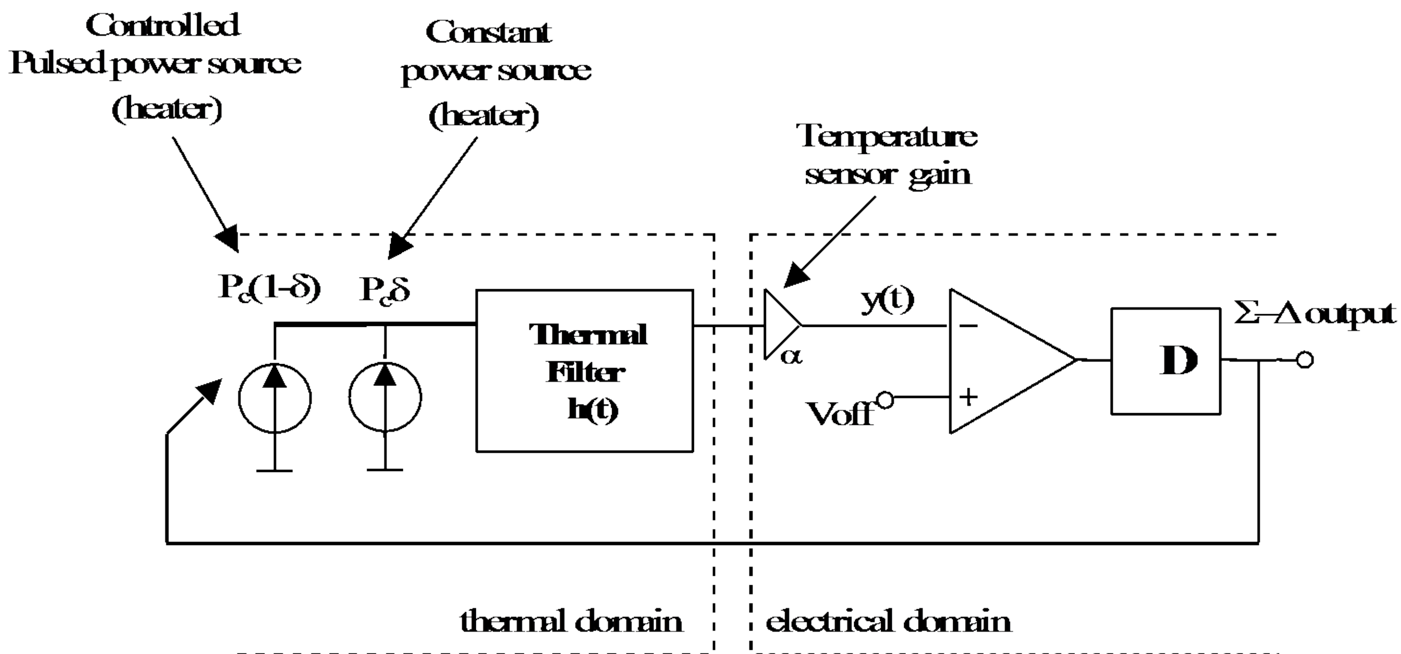
Controlled
Pulsed power source
(heater)
Constant
power source
(heater)
Temperature
sensor gain
$P_c(1-\delta)$
$P_c\delta$
Thermal
Filter
h(t)
α
y(t)
Voff
D
Σ–Δ output
thermal domain
electrical domain

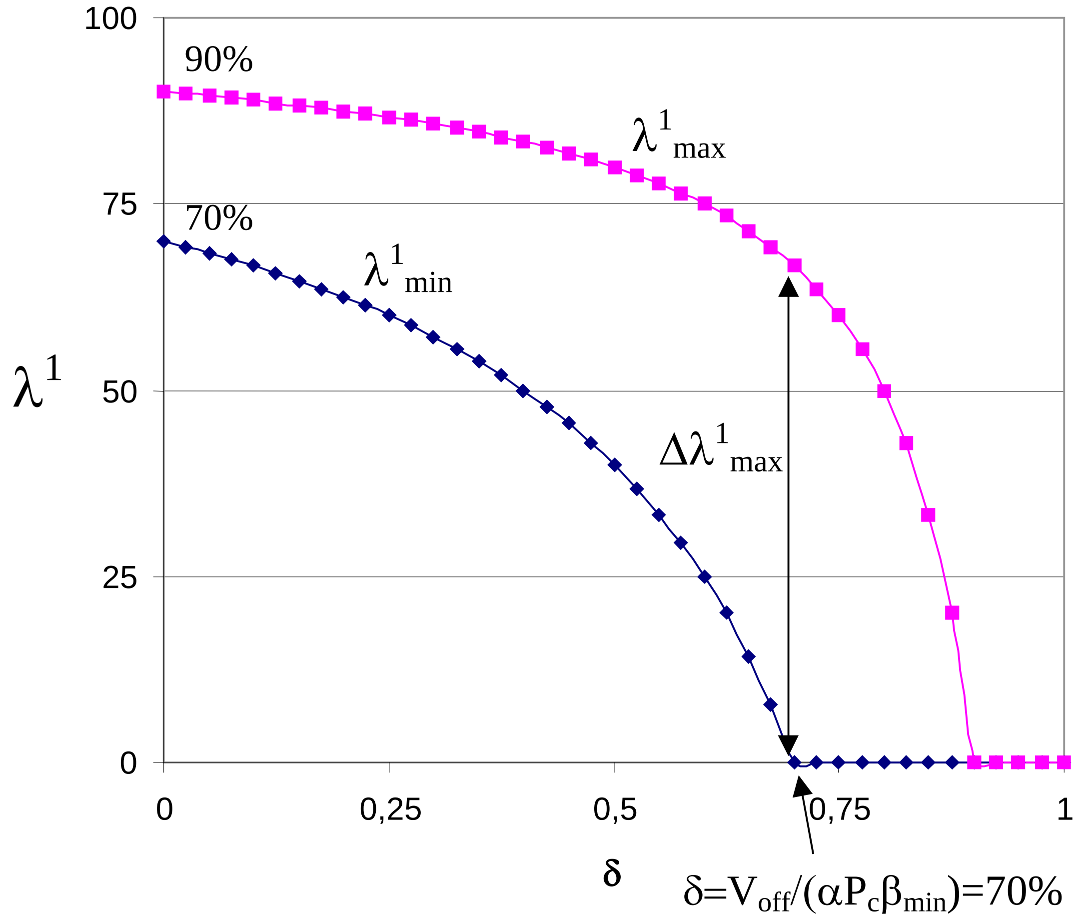
100
75
50
25
0
90%
70%
λ^1_{max}
λ^1_{min}
λ^1
$\Delta\lambda^1_{max}$
0
0,25
0,5
0,75
1
δ
$\delta = V_{off}/(\alpha P_c \beta_{min}) = 70\%$

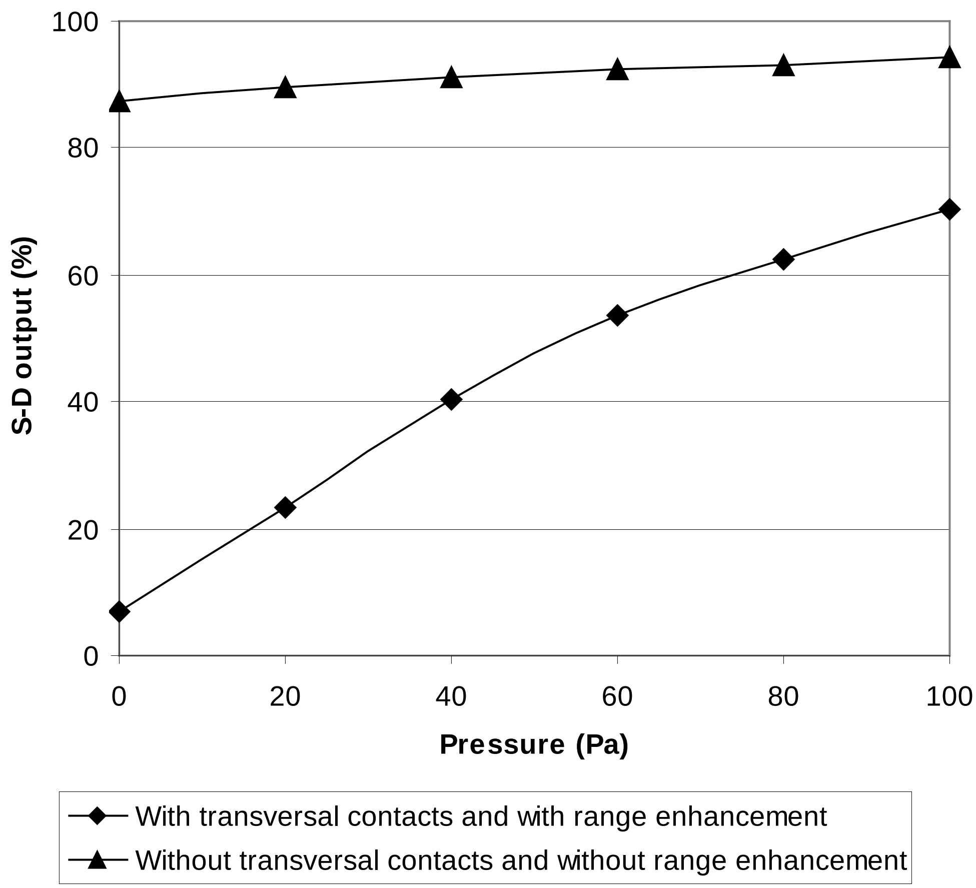

100
80
60
40
20
0
S-D output (%)
0
20
40
60
80
100
Pressure (Pa)
With transversal contacts and with range enhancement
Without transversal contacts and without range enhancement

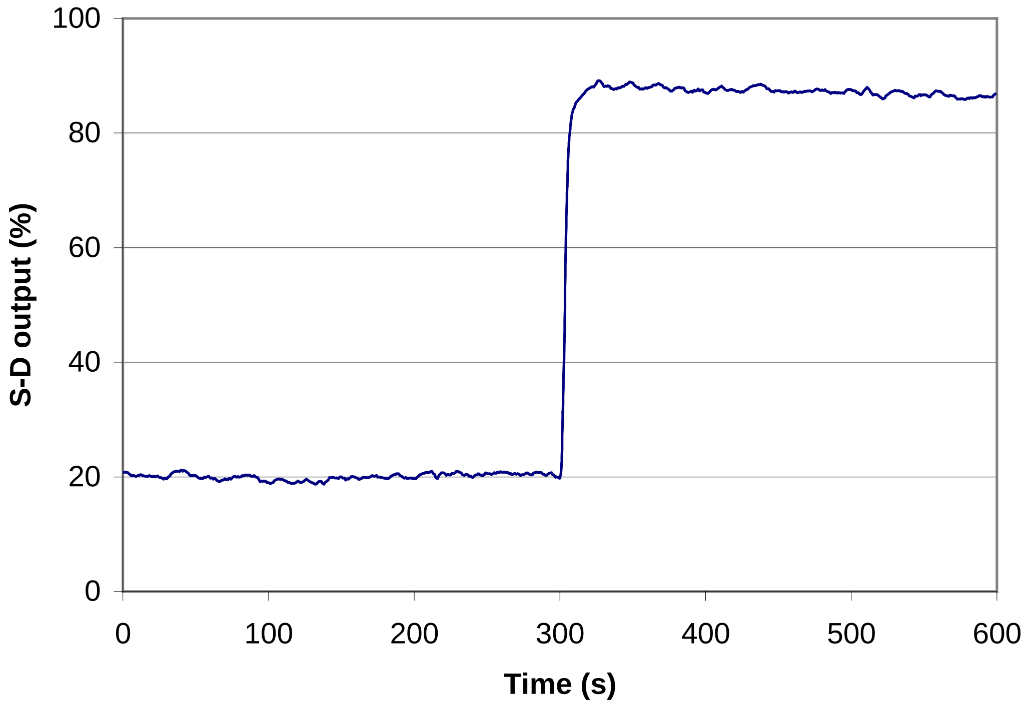

100
80
60
40
20
0
S-D output (%)
0
100
200
300
400
500
600
Time (s)

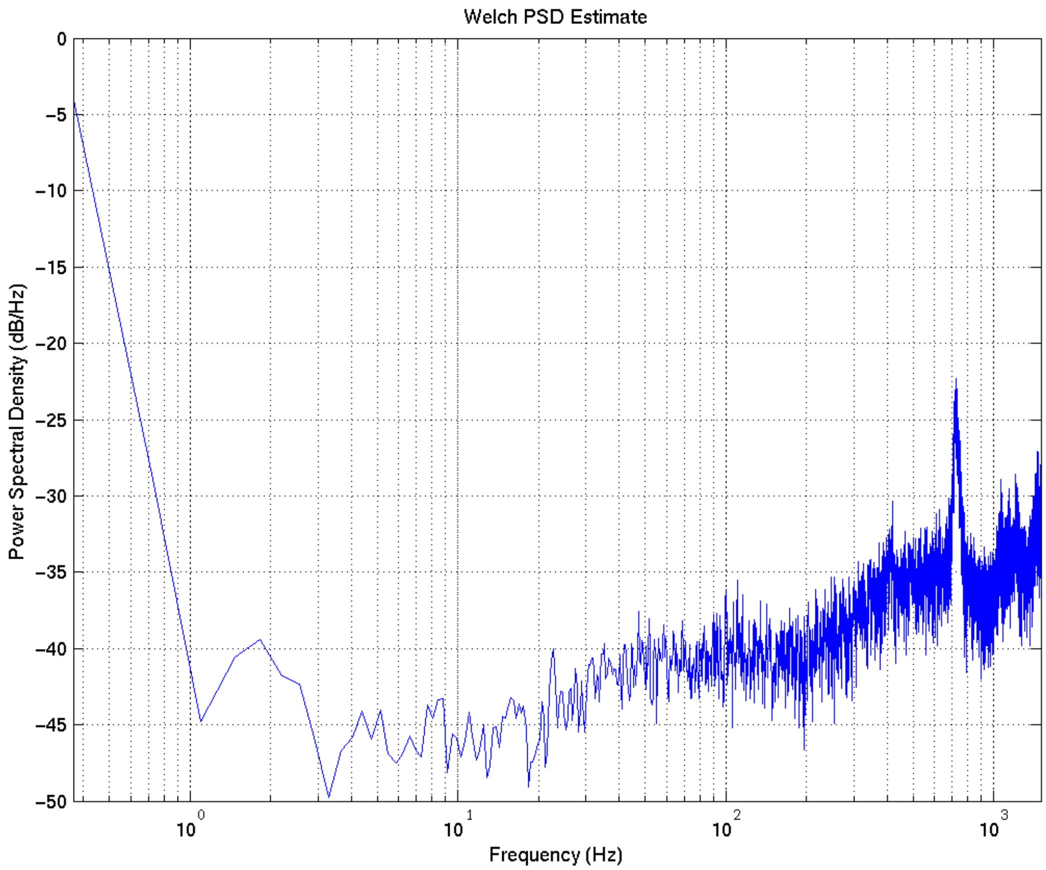
Welch PSD Estimate
Power Spectral Density (dB/Hz)
Frequency (Hz)
0
-5
-10
-15
-20
-25
-30
-35
-40
-45
-50
10^0
10^1
10^2
10^3

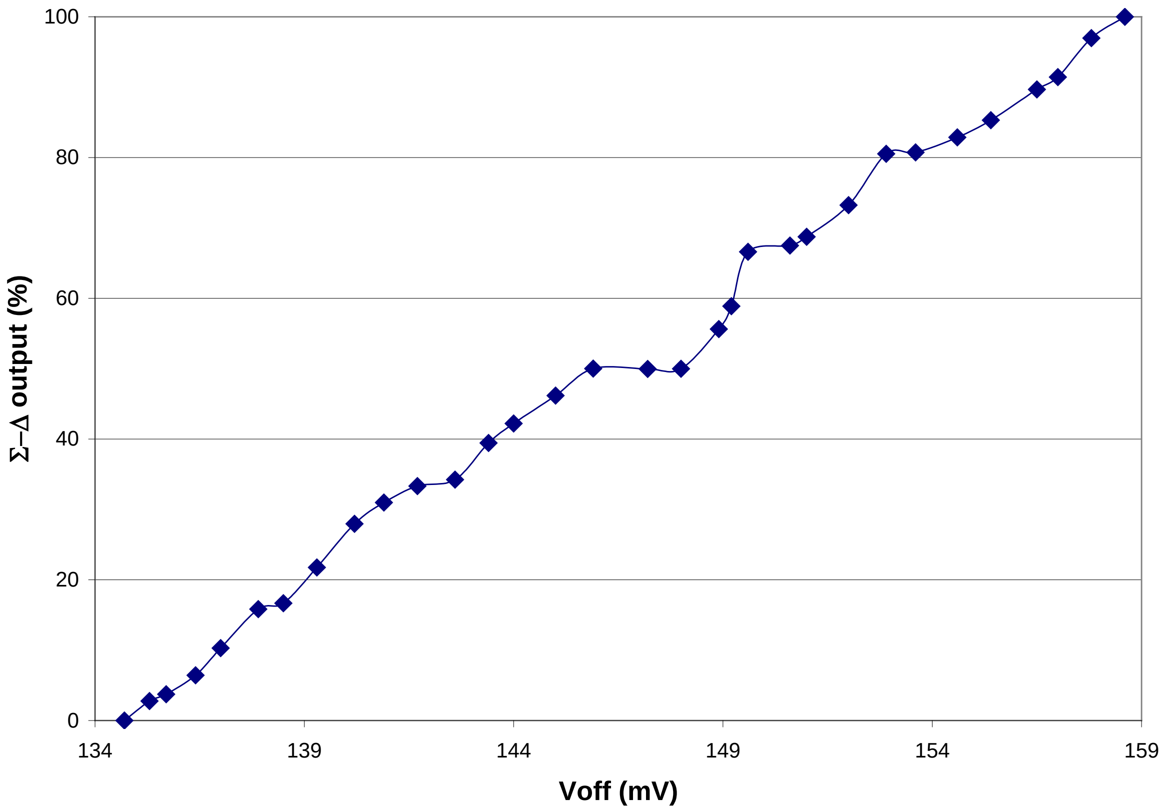

100
80
60
40
20
0
134
139
144
149
154
159
Σ–Δ output (%)
Voff (mV)